Anomalous phase transition of layered lepidocrocite titania nanosheets to anatase and rutile

Rodriguez, Paramaconi; Pu, Yayun; Chen, Qianwen; Sun, Zongzhao; Huang, Limin

DOI:
10.1021/acs.cgd.9b00147

Document Version
Peer reviewed version

Citation for published version (Harvard):
Rodriguez, P, Pu, Y, Chen, Q, Sun, Z & Huang, L 2019, 'Anomalous phase transition of layered lepidocrocite titania nanosheets to anatase and rutile', *Crystal Growth and Design*, vol. 19, no. 6, pp. 3298-3304. https://doi.org/10.1021/acs.cgd.9b00147

Anomalous phase transition of layered lepidocrocite titania nanosheets to anatase and rutile

Yayun Pu[1,2†], Qianwen Chen[2†], Zongzhao Sun[2], Paramaconi Rodriguez[1*] and Limin Huang[2*]

[1]School of Chemistry, University of Birmingham, Edgbaston, Birmingham B15 2TT, UK.

[2]Department of Chemistry, Southern University of Science and Technology, Shenzhen, 518055, China.

[†]These authors contributed equally.
[*]Corresponding author: P.B.Rodriguez@bham.ac.uk and huanglm@sustc.edu.cn

Abstract

In this study, phase transformations from lepidocrocite titania nanosheets (L-TiO_2) to rutile (R-TiO_2) and anatase (A-TiO_2) have been systematically investigated as a function of the preparation conditions, such as pH and freeze drying, and as a function of the temperature treatment. We have found that the transformation of (L-TiO2) into rutile takes place upon freeze drying treatment. We report that temperature determined the final phase-structure in the transition phase of the L-TiO_2 nanosheets into TiO_2 nanoparticles, while the pH determined the final morphology and particle size. Based on the experimental results, two different transition pathways of dissolution-recrystallization and topologically rolling transition have been proposed. Our results give a full map of phase transition and morphology evolution of L-TiO_2 to R-TiO_2/A-TiO_2 that can provide guideline to new materials design, especially for the photocatalysts.

Key words: two dimensional titania nanosheets, phase transition, hydrothermal treatment, anatase, rutile.

1. Introduction

Titanium oxides with various kinds of polymorphs, such as anatase, rutile, brookite and lepidocrocite-type layered structure, have been among the most studied material systems in energy relevant applications such as photoelectrochemical solar cells, photocatalysis and electrode materials for Li/Na-ion batteries.[1-7] To meet the ever-increasing energy demand, intensive efforts have been devoted to develop the titanium oxides with tunable compositions, morphologies and structures.[8-11] Understanding the properties of the materials as a function of the crystallographic structure and the phase transition amongst these polymorphs, *e.g.* the transformation of lepidocrocite-type TiO_2 nanosheets into rutile or anatase is essential to establish protocols of synthesis of these materials and their subsequent applications. Among the well-developed protocols, solution-based methods are suitable to control the size, morphology and crystallographic orientation of nanocrystals providing a broad spectrum of physical, chemical and electronic properties that have found interest in diverse areas.[12-14] For example, Pan *et al*. prepared specifically exposed facets anatase TiO_2 nanorod using the hydrothermal method and layered $Cs_{0.68}Ti_{1.83}O_4$ as precursor.[15] This materials found later application on dye-sensitized solar cells. The transition of layered titanate nanosheets to anatase at different pHs and above 100 ℃ was first reported by Wen *et al*.[16-17] The authors found that the formation of rutile is only favorable in strongly acidic environment (pH < 2). However, these studies do not provide a clear understanding of the phase transition and phase morphonology as the function of temperature and pH, thus there are still lack of a fully established transition map for an overall view. Energy relevant applications such as water splitting, solar conversation and lithium storage require precise control of the crystal phase, particles size, the special dominant facet and also the morphology, all of which are exclusively based on the complete

and deep understanding of such transition.

Here, this work provides a coherent and insightful investigation on the phase transition of titanium oxides polymorphs, featuring the dependence of temperature and pH change and with the aim of providing important information for the optimization parameters of dominant (101) facet of anatase single crystal, which is candidate material of photoanodes in photocatalytic hydrogen evolution and dot-sensitized solar cells (DSSC).

2. Methods

Preparation of layered lepidocrocite-type TiO_2 nanosheets suspension

The $Cs_xTi_{2-x/4}O_4$ precursor was prepared by a solid-state reaction according to previous report.[18] Typically, intimate mixture of titanium dioxide and a cesium carbonate (99.9% metals basis, Aladdin) with molar ratio of 1:5.3 were placed in a crucible and was heated at 800 ºC for 1 h for decarbonation. After cooling down, the powder was ground carefully and then was allowed for two cycles of heating at 800 ºC, 20 h. During that process, the powder was also ground four times. The as-synthetized $Cs_xTi_{2-x/4}O_4$ powder was then subjected to acidic exchange by 1 M HCl with solution-solid ratio of 100 cm^3/g. After 24 h, the solution was decanted and replaced by a fresh one. It was repeated 3 times. Obtained solid was filtered, rinsed with water 3 times and dried at 60 ºC. A weighed amount of $H_xTi_{2-x/4}O_4$ (0.1 g) was dispersed into 25 ml aqueous tetrabutyl ammonium hydroxide (TBAOH) solution (40 wt.%) under ultrasonic treatment for 4h, with H^+/TBA^+=1:5.

Hydrothermal treatment of colloidal suspension

First, 8mL of the L-TiO_2 nanosheet suspension was diluted in 24 ml of water and the pH was adjusted to pH=1, 3, 6 or 9 by HCl and TBAOH solution. In the following step, the TiO_2 nanosheet solution was transferred to a Teflon-lined stainless steel vessel with an internal volume of 50 ml. The reactor was sealed and kept for 24 h at different temperatures: 50 ºC, 80 ºC, 120 ºC, 180 ºC,

220 ºC. After the hydrothermal treatment, the product of the reactions was collected by centrifuging and was washed with distilled water five times. Finally, the nanoparticles s were dried in a conventional oven at 50 ºC overnight.

Freeze-drying steps were performed using two different protocols: *i)* freeze-drying was applied directly after centrifuging; or *ii)* a small amount of the samples were diluted with water after centrifuging, and then the freeze-drying step was applied.

Physicochemical and structural characterization

The samples were characterized by scanning electron microscopy (SEM, Zeiss, 15 kV) with energy dispersive X-ray spectroscopy (EDS) and transmission electron microscopy (TEM, FEI Tecnai F30, 300 kV). X-ray diffraction (XRD) patterns were acquired by the Rigaku Smartlab-9Kw X-ray diffractometer. Raman scattering spectra were collected by the confocal Lase Raman Spectrome (HORIBA LabRAM) with 532 nm He-Ne laser, a laser power of 1 mW was used to avoid sample damage, optimum exposure time (5 s) and multicycle (8) enhance the intensity that produce good quality spectra. Thermogravimetry analysis (TGA) was performed in the temperature range of 25-550 ºC by Shimadzu TGA-50 with a heating rate of 10 ºC /min, the nitrogen gas flow was 30 ml/min. The Differential Scanning Calorimeter (DSC) was performed using a Shimadzu DSC-60 Plus with a heating rate of 10 ºC /min, a nitrogen gas flow of 30 ml/min within the temperature window between 25-500 ºC. UV-Visible absorption spectra of the colloidal suspensions were recorded by Shimadzu UV-3101PC UV/Vis spectrometer. Zeta-potential data was obtained by the Zetasizer Nano ZS.

3. Results and discussion

The characterization of as-prepared lepidocrocite-type TiO_2 nanosheets (L-TiO_2) is presented in Figure 1. The SEM and TEM images show well-defined single layer nanosheets with an average

later size between 200-300 nm. The faded contrast in the TEM image and the AFM image in Figure S1 certify the molecular-level thickness (~1.5 nm) of the nanosheets.[18-19] Prior to the solvothermal treatment, the photochemical properties and stability of the colloidal solution of the exfoliated TiO_2 nanosheets were evaluated as a function of the pH by UV-Vis spectroscopy (Figure 1d) and the Zeta-potential (Figure 1e). As can be seen in figure 1d, the absorption peak at 266 nm is associated to the presence of colloidal suspension of polydisperse TiO_2 nanosheets, the peak weakens as the pH decreases from alkaline to acid until it disappears at pH=3. Such a decrease of the signal is directly associated to the accelerated flocculation of the suspension of nanoparticles in a range of pH between 5.0-6.0 (see optical image in Figure 1c). The flocculation of the nanoparticles can be explained in terms of the attractive and repulsive interaction of the particles and the surface charge as a function of the pH. As can be seen in Figure 1e, the Zeta-potential measurements reveal that the variation trend of exfoliated nanosheets on pH is similar to the UV-Vis spectra variation. Because of negatively charged surface of L-TiO_2, well dispersed nanosheets show a potential of -30 mV in alkaline conditions. The potential starts to change in the positive direction as the pH decreases, indicating that the nanosheets follow an accelerated assembly or restacking. At pH=3, the surface charge of the nanoparticles becomes positive, the Zeta-potential reaches a potential of +6 mV, suggesting the full restacking of the TiO_2 single-layer nanosheets. The change of the zeta potential and the change of charge is consistent with the precipitation process observed in the optical images and the trend observed on the UV-Vis spectra.

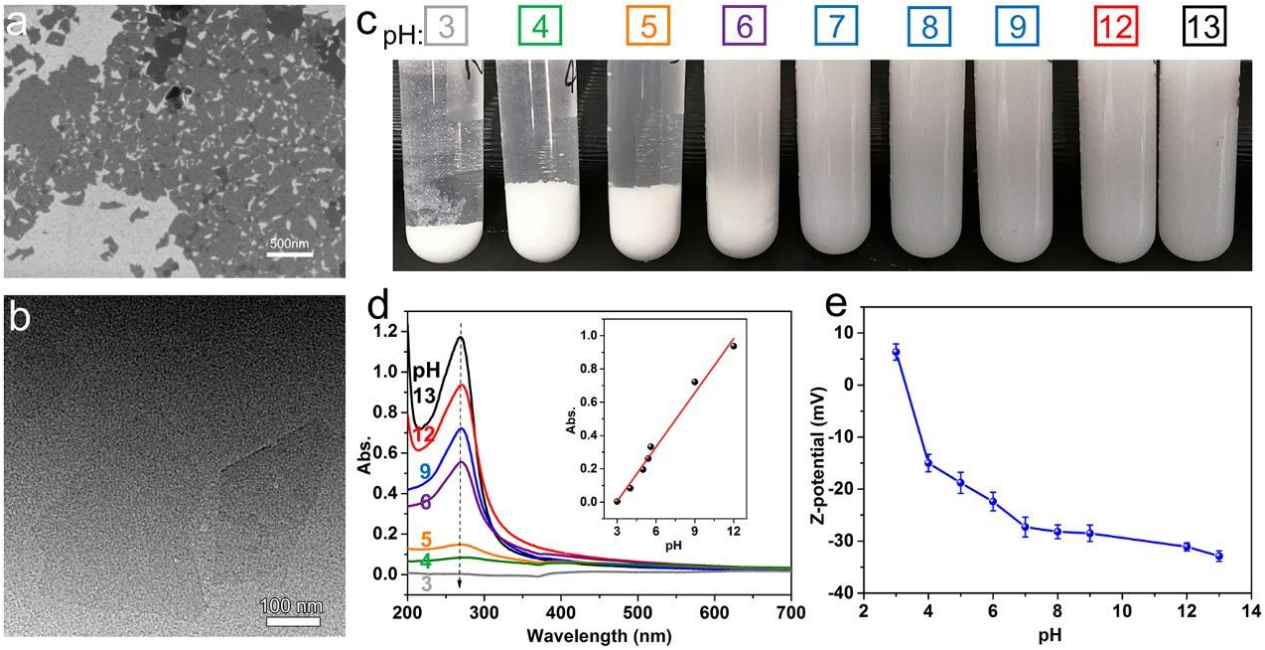

Figure 1. Characterization of L-TiO_2 nanosheets by a) SEM image and b) TEM image. Photographs of colloidal solution of of L-TiO_2 nanosheets at different pH (c) and their corresponding UV-Vis spectra (d) and Zeta-potentials (e). The inset in figure (d) corresponds to the plot of the intensity at 266 nm as a function of the pH.

Once the presence of exfoliated L-TiO_2 nanosheet and the stability of the suspension of the nanosheets as a function of the pH was confirmed, the hydrothermal phase transition of the nanosheets as a function of the temperature was evaluated at different pHs. The XRD patterns on figure S2 show no correlation between the phase transition and the pH, on the other hand this process is exclusively determined by the temperature. Evidence of the effect of the temperature on the phase transition is shown in figure 2. As can be seen in Figure 2a, L-TiO_2 nanosheets retain the 2D structure and restacked randomly in layered structure after the following freeze-drying protocol *(i)*. The signals at low angles $2\theta = 6.4^{o}$, 12.56^{o}, and 18.56^{o} are characteristic of reassembled nanosheets.[18] Following the freeze-drying protocol *(ii)*, unusual transition to rutile TiO_2 (R-TiO_2) can be indexed by diffraction peaks at $2\theta = 27.56^{o}$, 36.14^{o}, and 41.38^{o}, which correspond to (110),

(101), and (111) lattice plane (JCPDS 78-1509), respectively. As the temperature increases from 50 ºC to 180 ºC, XRD results clearly show how a new peak evolve at $2\theta = 25.4^{o}$ and the intensity further increases. In addition, the peaks at $2\theta = 27.56^{o}$, 36.14^{o} gradually weaken and finally disappear. When the temperature reaches 220 ºC, the peaks of the R-TiO_2 phase have completely disappeared and the pure anatase TiO_2 (A-TiO_2) phase is obtained. The signals at $2\theta = 25.4^{o}$, 37.9^{o} and 48.1^{o} correspond to the lattice planes of (101), (004), and (200) (JCPDS 73-1764), respectively.

The phase transition L-TiO_2 nanosheets as a function of the temperature observed by XRD was consistently confirmed using Raman spectroscopy (Figure 2b). In the Raman spectra of figure 2b, the bands observed at 143, 444 and 609 cm^{-1} are associated to B_{1g}, E_g and A_{1g} active modes of the R-TiO_2 phase. The signal at 240 cm^{-1} can be attributed to the two-phonon scattering mode[20] and the bands at 701 and 2930 cm^{-1} can be attributed to the incomplete conversion of L-TiO_2 nanosheets, as they are similar to the bands of the of the sample obtained after the freeze-drying protocol (*i*). In the temperature range from 50 ºC to 120 ºC, the main bands of samples remain unaltered, with the exception of the band at 143 cm^{-1} which gradually increases. This indicates that the main structure maintains as R-TiO_2 phase but A-TiO_2 phase starts to be form. Similar to the results obtained from XRD, as the temperature increases higher than 180 ºC, the bands at 444 cm^{-1} (E_g) and 609 cm^{-1} (A_{1g}) of the rutile phase becomes weaker, while the bands at 197, 395, and 515 cm^{-1} associated to the Raman active modes of E_g and B_{1g} of the A-TiO_2 phase[21] appear and their intensities increase as the temperature increases. Same as in the case of the XRD, no further changes were observed when the temperature reached 220 ºC, as the bands at 144, 197, 395, 515 and 635 cm^{-1} associated to the A-TiO_2 phase reached full intensity.

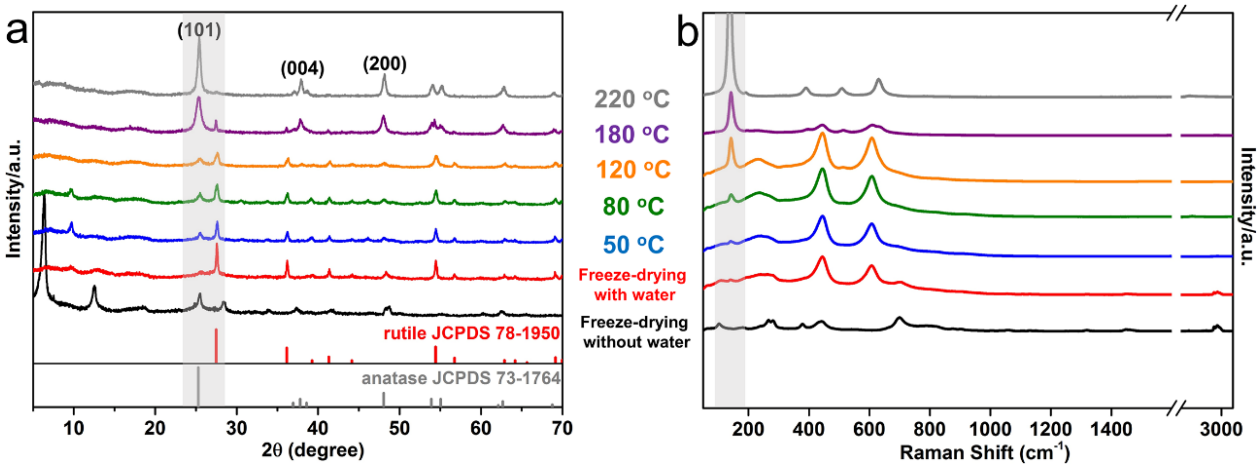

Figure 2. a) XRD diffraction patterns and b) Raman scattering spectra of hydrothermally treated L-TiO_2 nanosheets at pH=3 and at different temperatures as indicated in the figure.

TEM and SEM images of the samples were recorded in order to visualized the morphological changes of the TiO_2 nanostructures as a function of the temperature. Figure 3 shows electron microscopy images of the restacked L-TiO_2 nanosheets and nanoparticles obtained at 180 ºC hydrothermal treatment. As can be seen the pH of the synthesis strongly impact in the size and morphology of TiO_2 nanoparticles. The nanoparticles of the sample prepared in pH=3 show granular shape particles with diameter of ~30 nm (Figure 3d, g, j). On the other hand, both samples prepared in pH=6 and pH=9, shows A-TiO_2 nanoparticles with a rhomboid -like morphology and particles size of ~120 nm for the particles prepared in pH=9 and ~70 nm for those particles prepared in pH=6. This suggest that the phase transition and crystal growth is favored under alkaline conditions. A lattice spacing of 0.35 nm was determined from the HRTEM images of the A-TiO_2 nanocrystal particles prepared in pH=6 and pH=9. This lattice spacing corresponds to the plane (101) of anatase (Figure S4f) confirming the results obtained by XRD on Figure 2a.

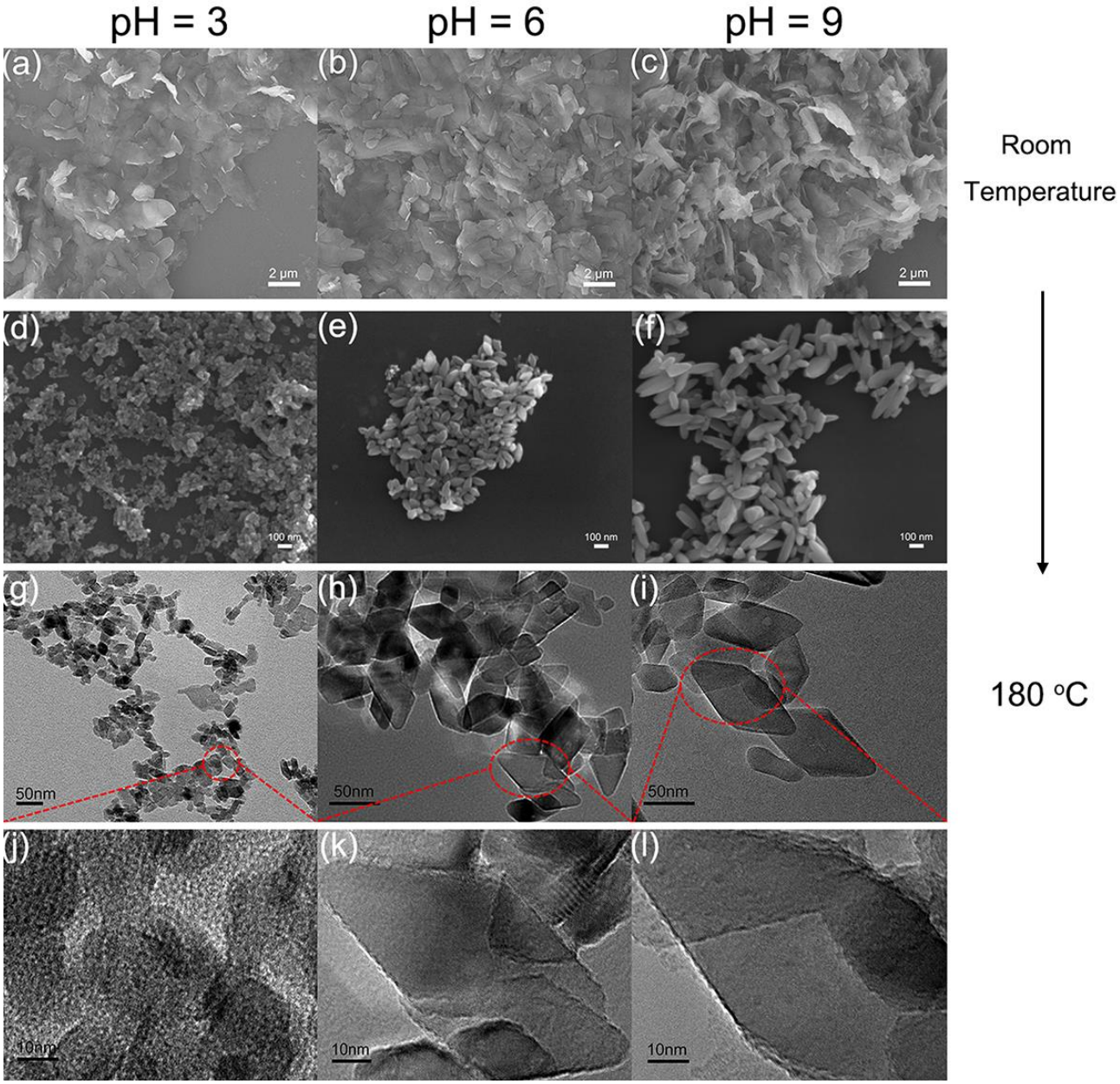

Figure 3. (a-f) **SEM images of stacked L-TiO_2 nanosheets and A-TiO_2 nanoparticles at different temperatures and pHs as indicated in the figure. (g-l) TEM images and HRTEM images of A-TiO_2 nanoparticles prepared at different pHs and after treatment at different temperatures as indicated in the figure.**

Based on these results, we propose two pH-dependence transition mechanisms of A-L-TiO_2 nanosheets towards the formation of other polymorphs of TiO_2 particles (Figure 4). In acidic media,

pH=3, the phase transition proceeds via a dissolution-recrystallization mechanism, while in neutral and alkaline media pH=6 and pH=9 the phase transition is controlled by a topological rolling mechanism. In the case of dissolution-recrystallization, nanosheets are restacked firstly and then dissolved in the solution under the harsh acidic environment. For example, as the annealing at 180 ºC proceeds, restacked small nanoplatelets with high free energy tend to dissolve into solution, which leads to a supersaturated solution of titanate. Then, A-TiO_2 starts to precipitate on the surface/edge of flake-like nanoplates (L-TiO_2) and grows up into small granular nanoparticles. Nanoplates eventually disappear and are totally transformed into A-TiO_2 nanoparticles with diameters between 30 to 50 nm. The transformation process of the nanoparticles prepared at pH=3 and annealed at 180 ºC as a function of time (6 h to 24 h) is shown in the SEM images on figure S5; the temperature dependence of the same nanoparticles is shown in Figure S6a, b, c. At pH=3, the A-TiO_2 nanoplates goes under structure transformation at 50 ºC due to dissolution. Such transformation process is enhanced even further at higher temperatures. At 80 ºC, the SEM images indicate a significant increase in the rugosity of nanoparticles and a gradual transformation of the nanoplates into round shape are observed. When the annealing temperature reaches 120 ºC, only smaller amorphous particles were observed in the SEM images. These evidence and poor crystallization of resulted A-TiO_2 nanoparticles confirmed by HRTEM image (Figure 3j) give strong support of such recrystallization process.

In the case of the samples prepared at neutral/alkaline pH (pH=6 to 9), the phase transition manner is dominated by the topological rolling mechanism.[17, 22] HRTEM and SEM images show highly oriented shuttle-like nanocrystals with large aspect ratio of length to thickness. The lattice spacing of d_{101} = 0.35 nm related to the (101) plane is the most preferentially exposed (Figure S4f). The XRD results (Figure 5) confirms that the L-TiO_2 precursor exhibit a typical interlayer plane of

(010), which is responsible for the (101) plane of resultant nanocrystals owing to topological rolling.[23] The temperature dependence of the nanoparticles is shown in Figure S6d-f. Two dimensional nanosheets with high surface energy could not maintain the well dispersion any more as being suffered from heat treatment but become splitting and rolling to reduce the Gibbs free energy. These smaller nanoplates are finally transformed into single nanocrystals via topologically rolling into shuttle-like particles, as shown in Figure 3.

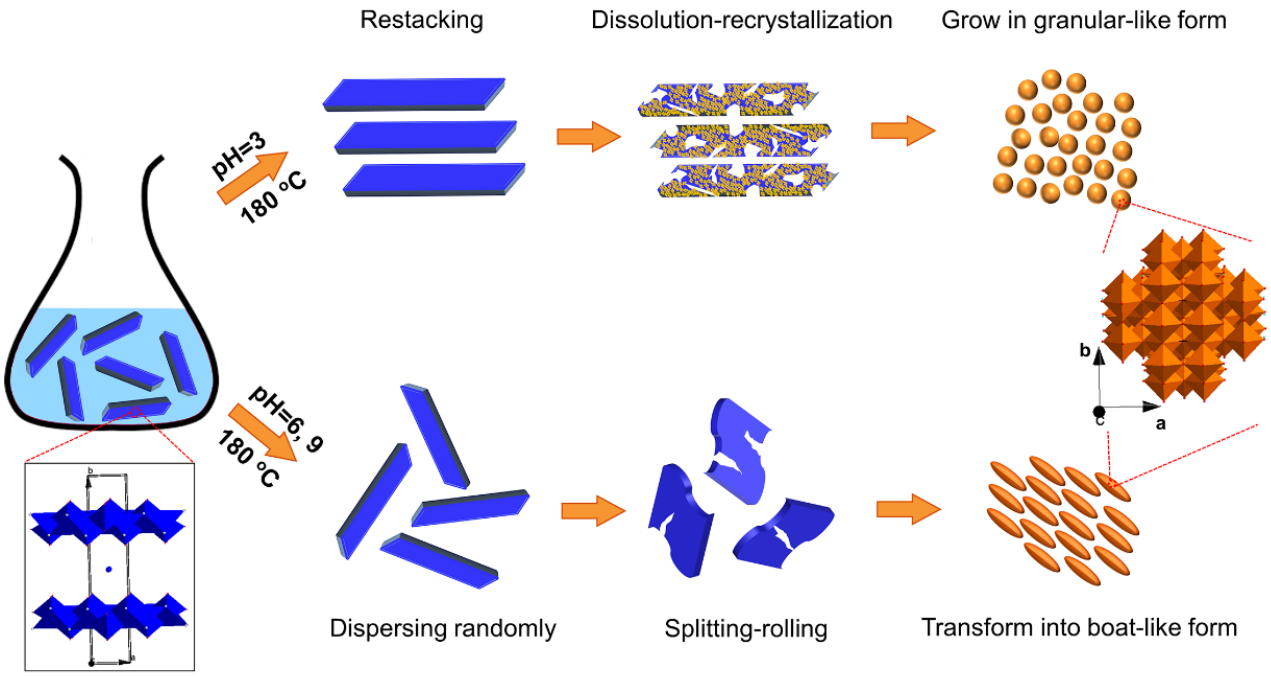

Figure 4. Schematic illustration for the pH-dependence transition mechanism of L-TiO_2 to A-TiO_2 nanoparticles.

To determine the role of the pH in the transition of the morphology of the L-TiO2 nanosheets, XRD (Fig. 5) and TGA (Fig. S7) of the initial L-TiO_2 nanosheets prepared at pH=3 and pH=6-9 were measured. Figure 5 shows the XRD patterns of exfoliated nanosheets suspensions being adjusted to different pH and then subjected to freeze-drying protocol (*i*). The signal at $2\theta \approx 5^{o}$, which corresponds to the (010) plane, clearly shows the dependence on pH that decreases with the

pH changing from alkaline to acid and indicates a change in the interlayer spacing of the nanosheets. From the shift of the peak, the interlayer distances between the nanosheets were calculated to be 17.1 Å for pH=12, 16.5 Å for pH=9, 14.8 Å for pH=6, 13.8 Å for pH=3 and 11.7 Å for pH=1. This suggests that the interlayer spacing increases as the pH increases allowing a larger intercalation of the TBA species.

The TGA curves in Figure S7, show that the initial mass decrease in the temperature range of 25 ºC to 200 ºC is similar for all the samples. These initial weight losses are associated to the desorption of water molecules. In the range between 200 ºC and 350 ºC, the samples prepared in acidic media (pH=3 and pH=1) rapidly lose up to 54% of mass. On the other hand, the samples prepared in neutral and alkaline media (pH=12, pH=9 and pH=6) lose steadily only 30 % of the total mass. This mass loss is due to the decomposition of TBA in the interlayer to trimethylamine and dimethyl ether.[24] The larger mass loss on the samples prepared at pH=1 and pH=3 in comparison to pH=6, pH=9, pH=12 indicates an increase of the amount of TBA intercalation in the samples prepared at lower pH. Interestingly, this result is contra intuitive as the XRD results show larger interlayer spacing in n the samples prepared at pH=6, pH=9, pH=12. The inversed results of the decrease of the interlayer spacing (XRD) and the increased intercalation of TBA ions (TGA) can be explained by accommodation of more TBA molecules in confined space in the interlayer (Fig. S7) and attributed to the molecule orientation and coulombic interactions.[25]

Based on the information above, the difference of transition mechanisms at pH=3 and pH=6-9 can be explained. At pH=3, the stability of stacked structure increases due to the increase of the coulombic interactions between the host L-TiO_2 layers and the TBA ions incorporated in the structure. This is directly associated to the decrease of the interlayer spacing and the larger TBA intercalation capacity. The high stability of the structure formed at pH=3 limit the spitting-rolling

mechanism and favor the dissolution and recrystallization mechanism. For the case of pH=6 and PH=9, well dispersion, weak interactions between host layers and sufficient space facilitate the expelling of TBA ions/water molecules and finally follow a topological transition mode.

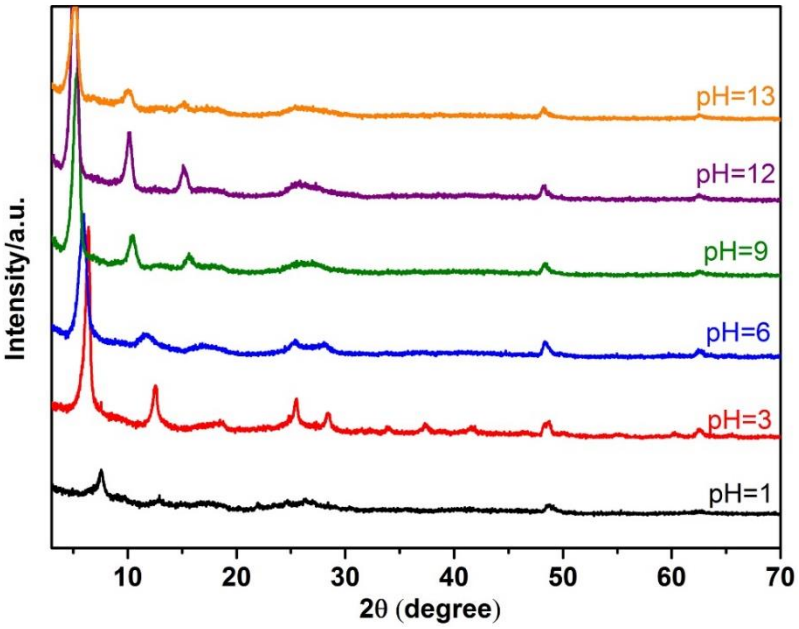

Figure 5. X-ray diffraction patterns of restacked L-TiO_2 nanosheets at different pH's.

4. Conclusion

In this study, phase transformation from L-TiO_2 nanosheets to R-TiO_2 and A-TiO_2 has been systematically investigated. Our study of the transition phase of the L-TiO_2 nanosheets as a function of temperature and pH reveals that the temperature determines the final phase-structure of the TiO_2 nanoparticles while the pH mostly influences the morphology and particle size.

It was found that 180 ^oC is a critical temperature that the resultant dominant phase is anatase. Under that condition, particles sizes increase with the pH increases from 3 to 9. The obtained A-TiO_2 particles in pH=3 solution are granular-like while in pH=6-9 are shuttle-like, in contrast to the initial sheet form L-TiO_2. Because the electron microscopy images and the XRD did not show significant differences in morphology for the samples prepared in pH=6 and pH=9, it is considered

the phase transition and morphology evolution follows the same mechanism. Two different transition pathways of dissolution-recrystallization and topologically rolling transition have been proposed to give detailed insight of such phase transition process. In acidic solution, pH=3, it follows the dissolution-recrystallization mechanism owing to the harsh corrosive environment and strengthened interlayer reaction between nanosheets. The strengthened interlayer reaction caused by decreased interlayer spacing and increased uptake of TBA ions is favorable to the stability of restacked structure. Thus, the L-TiO_2 precursor prefers to dissolution-recrystallization rather than topological rolling transition, which requires the individual nanosheets are dispersed well and can be rolling freely. Our results give a full map of phase transition and morphology evolution of L-TiO_2 to R-TiO_2/A-TiO_2 that can provide guideline to new materials design, especially for the photocatalysts such as dominant (101) facet anatase single crystal, which can be controllably synthesized according to our optimal parameters.

Acknowledgements

This work was financially supported by Southern University of Science and Technology (SUSTech) start fund through Shenzhen Peacock Talent program, the Basic Research Fund of Shenzhen (JCYJ20150507170334573), and Guangdong Innovative and Entrepreneurial Research Team Program (No.2016ZT06N532). P.R. acknowledges the University of Birmingham for financial support through the Birmingham fellowship program. This work was also supported by the Pico Center at SUSTech that receives support from Presidential fund and Development and Reform Commission of Shenzhen Municipality.

Notes

The authors declare no competing financial interest.

Supporting information

The Supporting Information is available free of charge on the ACS Publications website at DOI:

The supporting information includes: AFM profiles, UV vis spectrum, X-Ray patterns, HRTEM and SEM images, Thermogravimetric analysis.

References

1. Qin, D.-D.; Bi, Y.-P.; Feng, X.-J.; Wang, W.; Barber, G. D.; Wang, T.; Song, Y.-M.; Lu, X.-Q.; Mallouk, T. E., Hydrothermal growth and photoelectrochemistry of highly oriented, crystalline anatase TiO2 nanorods on transparent conducting electrodes. *Chem. Mater.* **2015,** *27*, 4180-4183.
2. Cho, I. S.; Choi, J.; Zhang, K.; Kim, S. J.; Jeong, M. J.; Cai, L.; Park, T.; Zheng, X.; Park, J. H., Highly efficient solar water splitting from transferred TiO2 nanotube arrays. *Nano Lett.* **2015,** *15*, 5709-5715.
3. Li, R.; Weng, Y.; Zhou, X.; Wang, X.; Mi, Y.; Chong, R.; Han, H.; Li, C., Achieving overall water splitting using titanium dioxide-based photocatalysts of different phases. *Energy & Environmental Science* **2015,** *8* , 2377-2382.
4. Li, Z.; Luo, W.; Zhang, M.; Feng, J.; Zou, Z., Photoelectrochemical cells for solar hydrogen production: current state of promising photoelectrodes, methods to improve their properties, and outlook. *Energy & Environmental Science* **2013,** *6* , 347-370.
5. Han, M. H.; Gonzalo, E.; Singh, G.; Rojo, T., A comprehensive review of sodium layered oxides: powerful cathodes for Na-ion batteries. *Energy & Environmental Science* **2015,** *8*, 81-102.
6. Tsiamtsouri, M. A.; Allan, P. K.; Pell, A. J.; Stratford, J. M.; Kim, G.; Kerber, R. N.; Magusin, P. C.; Jefferson, D. A.; Grey, C. P., Exfoliation of layered Na-ion anode material Na2Ti3O7 for enhanced capacity and cyclability. *Chem. Mater.* **2018,** *30*, 1505-1516.
7. Zhang, J.; Zhou, P.; Liu, J.; Yu, J., New understanding of the difference of photocatalytic activity among anatase, rutile and brookite TiO2. *Phys. Chem. Chem. Phys.* **2014,** *16*, 20382-20386.
8. Lawrence, M. J.; Celorrio, V.; Shi, X.; Wang, Q.; Yanson, A.; Adkins, N. J.; Gu, M.; Rodríguez-López, J.; Rodriguez, P., Electrochemical Synthesis of Nanostructured Metal-doped Titanates and Investigation of Their Activity as Oxygen Evolution Photoanodes. *ACS Applied Energy Materials* **2018,** *1*, 5233-5244.
9. Bilmes, S.; Mandelbaum, P.; Alvarez, F.; Victoria, N., Surface and electronic structure of titanium dioxide photocatalysts. *The Journal of Physical Chemistry B* **2000,** *104*, 9851-9858.
10. Lawrence, M. J.; Kolodziej, A.; Rodriguez, P., Controllable synthesis of nanostructured metal oxide and oxyhydroxide materials via electrochemical methods. *Current Opinion in Electrochemistry* **2018,** 10, 7-15.
11. Kromer, M. L.; Monzo, J.; Lawrence, M. J.; Kolodziej, A.; Gossage, Z. T.; Simpson, B. H.; Morandi, S.; Yanson, A.; Rodríguez-López, J.; Rodríguez, P., High-Throughput Preparation of Metal Oxide Nanocrystals by Cathodic Corrosion and Their Use as Active Photocatalysts. *Langmuir* **2017,** *33* , 13295-13302.
12. Zhao, B.; Lin, L.; He, D., Phase and morphological transitions of titania/titanate nanostructures from an acid to an alkali hydrothermal environment. *Journal of Materials Chemistry A* **2012,** *1*, 1659-1668.
13. Zhu, H. Y.; Lan, Y.; Gao, X. P.; Ringer, S. P.; Zheng, Z. F.; Song, D. Y.; Zhao, J. C., Phase Transition between Nanostructures of Titanate and Titanium Dioxides via Simple Wet-Chemical Reactions. *J. Am. Chem. Soc.* **2005,** *127*, 6730-6736.
14. Yuan, H.; Besselink, R.; Liao, Z.; Johan, E., The swelling transition of lepidocrocite-type protonated layered titanates into anatase under hydrothermal treatment. *Scientific reports* **2014,** *4*, 4584.
15. Pan, J.; Wu, X.; Wang, L.; Liu, G.; Lu, G. Q.; Cheng, H. M., Synthesis of anatase TiO2 rods with dominant reactive {010} facets for the photoreduction of CO2 to CH4 and use in dye-sensitized solar

cells. *Chem. Commun. (Camb.)* **2011,** *47*, 8361.
16. Wen, P.; Itoh, H.; Tang, W.; Feng, Q., Single nanocrystals of anatase-type TiO2 prepared from layered titanate nanosheets: Formation mechanism and characterization of surface properties. *Langmuir* **2007,** *23*, 11782-11790.
17. Wen, P.; Ishikawa, Y.; Itoh, H.; Feng, Q., Topotactic Transformation Reaction from Layered Titanate Nanosheets into Anatase Nanocrystals. *The Journal of Physical Chemistry C* **2009,** *113, 20275–20280*.
18. Sasaki, T.; Watanabe, M.; Hashizume, H.; Yamada, H.; Nakazawa, H., Macromolecule-like aspects for a colloidal suspension of an exfoliated titanate. Pairwise association of nanosheets and dynamic reassembling process initiated from it. *J. Am. Chem. Soc.* **1996,** *118*, 8329-8335.
19. Sasaki, T.; Watanabe, M., Semiconductor nanosheet crystallites of quasi-TiO2 and their optical properties. *The Journal of Physical Chemistry B* **1997,** *101*, 10159-10161.
20. Zhang, J.; Li, M.; Feng, Z.; Chen, J.; Li, C., UV Raman Spectroscopic Study on TiO2. I. Phase Transformation at the Surface and in the Bulk. *The Journal of Physical Chemistry B* **2006,** *110*, 927-935.
21. Ohsaka, T.; Izumi, F.; Fujiki, Y., Raman spectrum of anatase, TiO2. *J. Raman Spectrosc.* **1978,** *7* , 321-324.
22. Yuan, H.; Besselink, R.; Liao, Z.; Ten Elshof, J. E., The swelling transition of lepidocrocite-type protonated layered titanates into anatase under hydrothermal treatment. *Sci Rep* **2014,** *4*, 4584.
23. Ma, R.; Yoshio Bando, A.; Sasaki, T., Directly Rolling Nanosheets into Nanotubes. *Cheminform* **2004,** *35*, 2115-2119.
24. Musker, W. K., A reinvestigation of the pyrolysis of tetramethylammonium hydroxide. *J. Am. Chem. Soc.* **1964,** *86*, 960-961.
25. Sasaki, T.; Izumi, F.; Watanabe, M., Intercalation of pyridine in layered titanates. *Chem. Mater.* **1996,** *8*, 777-782.

For Table of Contents Use Only

Anomalous phase transition of layered lepidocrocite titania nanosheets to anatase and rutile

Yayun Pu[1,2†], Qianwen Chen[2†], Zongzhao Sun[2], Paramaconi Rodriguez[1*] and Limin Huang[2*]

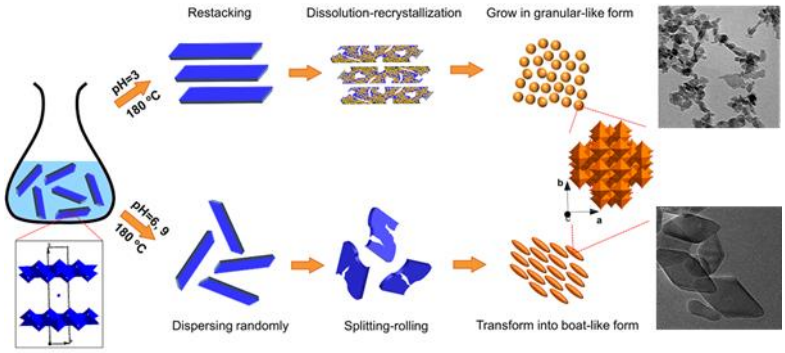

Our study of the transition phase of the L-TiO_2 nanosheets as a function of temperature and pH reveals that the temperature determines the final phase-structure of the TiO_2 nanoparticles while the pH mostly influences the morphology and particle size.